3D Physics-Based Registration of 2D Dynamic MRI Data

Raffaella Trivisonne, Igor Peterlik, Stéphane Cotin, Hadrien Courtecuisse

3D Physics-Based Registration of 2D Dynamic MRI Data

Raffaella TRIVISONNE [a,b] Igor PETERLIK [b,c] Stéphane COTIN [b]
Hadrien COURTECUISSE [a,b]

[a] *CNRS Strasbourg and Strasbourg University*
[b] *Inria Nancy and Strasbourg University, IHU Strasbourg*
[c] *Institute of Computer Science, Masaryk University, Brno, Czech Republic*

Abstract.
We present a method allowing for intra-operative targeting of a specific anatomical feature. The method is based on a registration of 3D pre-operative data to 2D intra-operative images. Such registration is performed using an elastic model reconstructed from the 3D images, in combination with sliding constraints imposed via Lagrange multipliers. We register the pre-operative data, where the feature is clearly detectable, to intra-operative dynamic images where such feature is no more visible. Despite the lack of visibility on the 2D MRI images, we are able both to determine the location of the target as well as follow its displacement due to respiratory motion.

Keywords. FEM, Non-Rigid Registration, Dynamic MRI, Robotic assistance

1. Introduction and Context

Medical imaging is by now one of the essential aspects to perform most of the ordinary daily surgeries. It represents not only a support for diagnostics, but also an actual operative instrument during particular therapeutic procedures. Typically, tomography techniques (CT and MRI) guarantee better results due to their accuracy into tissues differentiation and the consequent amount of information provided. In order to exploit the precision and the efficiency of these techniques, and to optimize as well the working environment for the operators, new procedures have been developed involving the combined use of tomography and robotic systems. So far it has concerned mainly percutaneous interventions, spacing from cryoablation for prostate cancer to neurosurgical applications.

Each technique presents its benefits and drawbacks: CT scans are faster and can provide particularly detailed anatomical representations of high contrasted organs; on the other hand they involve X-rays absorption. MRI images, being based on magnetism, do not have any absorbed dose, moreover they offer an excellent contrast of soft tissues; the main disadvantages are the length of the procedure as well as the necessity of totally non-ferromagnetic equipment. From a physiological point of view, organs are not static objects and even the simplest breathing motion can induce shape deformations. These modifications may invalidate the preoperative planning since the location of internal structures may significantly vary. Modern MRI allow for dynamic scanning without

any artifacts due to movement, but it is for now restricted to only one plan of acquisition. Therefore, given the absence of any volumetric information, some anatomical structures might be excluded. In this paper we extend the method presented in [4]. We aim to target an inflame porcine gallbladder as during as a robotic MRI-guided percutaneous procedure. We show that 3 orthogonal MRI slices are sufficient to perform an entire 3D registration of a preoperative segmented CT scan. Lastly, as the dynamic motion of the liver can only be acquired along a single plan at time, we show how to combine static slices with a single dynamic acquisition in order to provide an entire volumetric interpolation of the breathing motion.

2. Literature Review

The advantages of surgical robots and manipulators are well recognized (from daily assistance to telesurgery) [5]. In particular, MRI compatible robots are being developed for biopsies [13], prostate cancer [1] and even neurosurgical applications [10]. Typically, at the beginning of the intervention, clinicians select a couple of images and manually define a trajectory and some landmarks, in order to fix an entry point, a needle orientation and an approximative path. The robotic system will then semi-automatically proceed towards the target following the set trajectory. One remaining limitation is that initially chosen images may be suitable to plan needle insertion but far from the target. A real-time system tracking is then necessary to specifically take into account all the deformations caused by external forces or natural motions (such as breathing) [12].

Augmented Reality is an active research area which allows overlaying key informations on the top of medical images, such as the location of a tumor. It is a promising technique for mini invasive surgery assistance as well as for robotic-assisted procedures [7]. Most of augmented reality systems are still limited to rigid registration, but it has been reported (for instance for the liver motion) that purely rigid transformation is not sufficient for most of the surgeries. Recently, biomechanical models have been used for their ability to regularize the ill-posed non rigid registration problem. [8] uses a Finite Element model and the iterative closest point (ICP) algorithm for the registration of muscular structures. [14] proposed a physics-based shape matching (PBSM) method based on an electrostatic formulation. An elastic body is electrically charged to slides toward an oppositely charged rigid shape. [2] formulated the non rigid registration problem as an inverse mechanical problem. The method provides a set of boundary conditions bringing the FE model to the desired geometrical deformations.

The above methods require a complete segmentation of intraoperative surfaces but, as stated above, dynamic MRI acquisition is only possible along a single orientation at a time. In [9], the boundary of the liver surface is extracted and tracked from a laparoscopic camera during the intervention, but the tracking method may occur into camera occlusions. [6] use a linear elastic FE model of the brain that is driven by active surface matching of one acquired image during brain shift, but no significant dynamic motion are taken into account. In [4] a 3D volume is registered with 3 orthogonal sequences of dynamic MRI recorded one after an other and synchronized manually. We propose an extension of this method where a single dynamic slice is combined with static MRI slices. The main contributions of this work are: register a generic organ with missing complete volumetric information, target an anatomical feature not visible in MRI images, and perform all these operations with a combination of dynamic and static mode.

3. Methodology

The tracking method takes as input: an initial 2D segmentation of the liver's outline and a continuous flow of dynamic MRI slices. The initial segmentation is manually performed by an operator (fig. 1(a)), thanks to highly contrasted MRI images, this operation is easily performed and can be even more facilitated with the use of a tactile device (1(b)). The outline of the segmentation is then discretized providing a set a sparse control points located on the surface of the liver (see 1(c)).

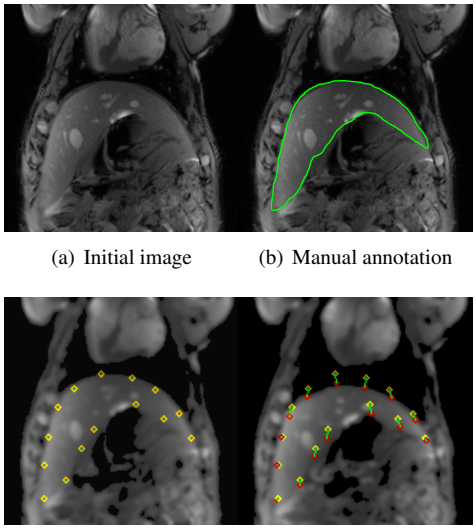

(a) Initial image (b) Manual annotation

(c) Image filtering (d) Outline tracking

Figure 1. We manually defined the contour of the liver applying some filters to enhance the quality of the image and we used OpenCV library to track the contour (in red) in the sequence of dynamic 2D MRI slices

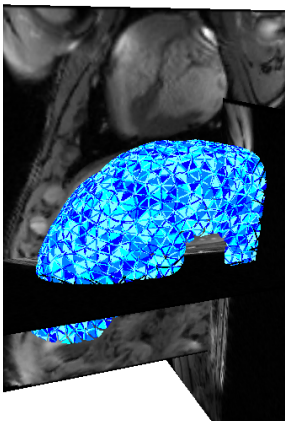

Figure 2. FE collision model of the liver

The MRI MAGNETOM® Aera SIEMENS 1.5 T allows to get, in dynamic mode, 2.5 acquisitions per second of a given slice. This frequency is sufficient to capture the dynamic behavior of tissues during breathing cycles without any artifacts due to organs' motion. In order to reduce the noise, both a Gaussian and a Threshold filter are applied to the acquired the images (see 1(c)). An optical flow algorithm provided by OpenCV is then used to track the displacement of the liver's initial boundary in the dynamic sequence (see Fig. 1(d)). Finally, based on the position and orientation of the MRI slices, a set of sparse 3D control points $\mathbf{p}$ located on the liver's surface can be reconstructed. The porcine liver and its gallbladder have been segmented from a preoperative CT scan; a tetrahedral mesh was generated to support FE computations (see Fig. 2).

We use the corotational FE approach [11] to deal with non-linear deformations. The deformation of the model is given by the dynamic equation:

$$\mathbf{M}\ddot{\mathbf{q}} + \mathbf{B}\dot{\mathbf{q}} + \mathbb{F}(\mathbf{q}, \dot{\mathbf{q}}) + \mathbb{H}(\mathbf{q}, \mathbf{p}, \lambda) = 0 \tag{1}$$

where $\mathbb{F}(\mathbf{q},\dot{\mathbf{q}})$ are internal volumes forces for given positions $\mathbf{q}$ and velocities $\dot{\mathbf{q}}$. $\mathbf{M}$ and $\mathbf{B}$ are respectively the mass and the damping matrices. $\mathbb{H}(\mathbf{q},\mathbf{p},\lambda)$ gathers the constraints forces λ for given positions $\mathbf{q}$ and $\mathbf{p}$.

The location of the corresponding control points $\mathbf{p}$ on the liver's surface is not known. This problem is solved employing the Iterative Closest Point (ICP) method as described in [4]. At the beginning of each simulation step, each control point is associated with its respective nearest triangle on the surface of the segmented liver. We assume that this association stays constant within a simulation step (see [3] for details), allowing to define the Jacobian of Constraints $\mathbf{J}$ and the violation of constraint $\delta = \mathbf{p} - \bar{\mathbf{q}}$, defined as the distance between $\mathbf{p}$ and its respective closest projection on liver's surface $\bar{\mathbf{q}}$:

$$\begin{cases} \mathbf{M}\ddot{\mathbf{q}} + \mathbf{B}\dot{\mathbf{q}} + \mathbb{F}(\mathbf{q},\dot{\mathbf{q}}) + \mathbf{J}\,\lambda = 0 \\ \mathbf{J}^T\,\bar{\mathbf{q}} = \delta \end{cases} \tag{2}$$

Due to off-plan motions, tracked points may not be associated with the same positions on the liver's surface. We use then sliding constraints (see [4]) allowing the FE model to slide around the configuration, minimizing the mechanical energy needed to perform the registration. A normal direction $\mathbf{n}$ is associated to each constraint from Bezier subdivision of liver triangulation surface. After the resolution, λ is computed such that no violation remains in $\mathbf{n}$-direction ($\delta = 0$), with any tangential force.

A Backward Euler implicit time integration is used to perform the simulation. It involves a non-linear problem solved with a single iteration step of the Newton solver. After the linearization, the problem is written as an augmented linear system: $\mathbf{A}\mathbf{x} + \mathbf{J}\lambda = \mathbf{b}$ where $\mathbf{A} = \frac{1}{h}\mathbf{M} + \mathbf{B} + h\frac{\partial \mathbb{F}}{\partial \mathbf{q}}$, $\mathbf{x}$ and $\mathbf{b}$ being respectively the increment and residual in the Newton solver (see [3] for details). The Schur complement method is used to solve the augmented linear system, involving the computation of the *compliance matrix* $\mathbf{W} = \mathbf{J}\mathbf{A}^{-1}\mathbf{J}^T$ that relates the mechanical coupling between constraints.

The constrained problem has a solution if and only if all the constraints are exactly verified at the end of each simulation step. However, the tracking method may generate outliers resulting in a non physically plausible deformation. To avoid excessive deformations of the biomechanical model, a soft compliance factor $\mathbf{W}^{\text{soft}}$ is added to the compliance matrix: $(\mathbf{W} + \mathbf{W}^{\text{soft}})\,\lambda - \delta = 0$, where $\mathbf{W}^{\text{soft}}$ is a diagonal matrix whose coefficients are directly related to the confidence of the tracking method. Instead of deforming the FE liver model, higher compliance allows moving outliers on liver's surface if the necessary energy is be too high to satisfy the constraint. Thanks to variations in compliance it is possible to combine dynamic constraints with static ones.

4. Results

In order to validate our method, we evaluate the error between the registered mesh and its actual position into MRI images; this error is calculated as the distance between the surface of the registered mesh and some control points outlining the contour of each anatomical feature on MRI images.

To have the information as global as possible, we acquired MRI dynamic data along 9 different orientations. Given an average porcine respiratory rate of 15-20 breaths per minute and an MRI-acquisition frequency of 0.4 Hz for each dataset we selected the 10 images corresponding to a single breathing cycle. Such slices have been then syn-

Slices	Outline average [mm]	Gallbladder average [mm]
C_0	8.8	10.5
A_0	15.8	10.6
S_0	6.6	5.81
C_0 A_0 S_0	2.0	3.9
C_0 A_0 S_{max}	1.7	1.5
C_0 A_0 S_{min}	1.9	1.7
C_0 A_{max} S_0	2.5	10.6
C_0 A_{min} S_0	7.4	9.7
C_{max} A_0 S_0	3.2	5.9
C_{min} A_0 S_0	2.0	1.4

Table 1. Average distance between registered mesh and control points on MRI images

chronized setting as init the slice corresponding to the maximum inspiration and control points have been selected onto starting image.

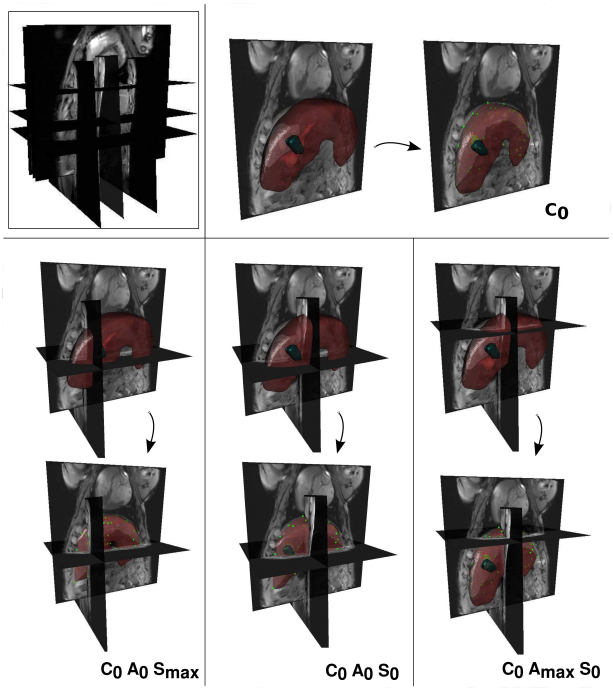

Figure 3. Examples of constraints configurations. We captured 9 MRI-images along coronal, sagittal, and axial plan in order to roughly span the whole abdominal volume (image top left). We combined the slices in order to create configurations of constraints with different orientations. The notation C_i A_i S_i indicates the slices and their level within the abdominal volume (*0* center, *max* proximal, *min* distal) Figures show the registration testing different configurations. Validation points change color according to the registration's result: the greener they are, the more the mesh is close to such control points. In general, a constranints configuration could be working for the liver but not for the gallbladder (i.e. C_0 A_{max} S_0, image bottom right)

For the static part, each test was performed activating a set of 3 different constraints at once, while the control points for the validation distance were considered in the whole area. For each test, we registered the liver changing one constraint (i.e. MRI-slice) per time; in particular, we chose the most external ones (*min,max*), defining the boundary of our volume. Results of the average error of gallbladder and liver registration, as well as the configuration of the slices, are shown in (Fig. 3).

Outcomes are rather satisfying: average deviations float around 2 mm, except for the combination of constraints the distal axial slice. In order to achieve optimal results, two criteria must be fulfilled by a constraint: it must be set on a region with high volume density and it has to present a not generic contour." In this case, such axial image, not only belongs to a restricted portion of the liver, but its outline doesn't give enough information about the shape. The best result is achieved with the combination of central coronal, central axial and proximal sagittal. Furthermore, we show how a combination of three slices is preferable in respect of a single constraint (Tab. 1).

We performed dynamic tests using the best constraints-combination deriving from static tests (i.e. C_0 A_0 S_{max}). Each real-time simulation was performed for 16s to record at least 4 breathing cycles; picks in (Fig. 4 represents maximum inspiration phase. We proposed a registration combining dynamic and static slices, despite our method could give good results using three dynamic constraints at the same time (fig. 4); we chose such heterogeneous configuration since a configuration with three dynamic orthogonal plans is not clinically realizable yet. However, the choice of the dynamic slice should still respect criteria of included volume's percentage and outline's specificity: the combination C_0 A_0 S_{max} with the coronal slice in dynamic mode, is the one giving the smallest deviation. In general, such dynamic/static combinations are possible applying an higher compliance to static slices, in order to let control points move more easily. Lastly, we tested t fourth combination of three static constraints: as shown in (Fig. 4), in case of breathing a static registration would give a more significant error.

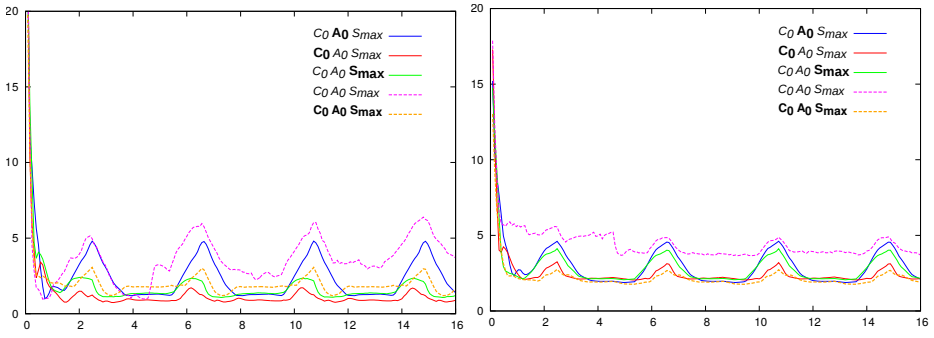

(a) Gallbladder Average Error

(b) Outline Average Error

Figure 4. Average errors between registered surface and image control points during dynamic registrations. Here we show the results for both the liver and the gallbladder when using different combinations. With the static combination C_0 A_0 S_{max} is hard to follow the breathing motion; the dynamic combination $\mathbf{C}_0$ $\mathbf{A}_0$ $\mathbf{S}_{max}$ shows good results, yet it's not clinically useful; the best configuration is $\mathbf{C}_0$ A_0 S_{max} where only the coronal slice is in dynamic mode. The registration process is generally completed after 6-7s for all the combinations, as shown in the x-axis. After this first phase, errors tend to be stationary with an oscillatory pattern due to respiratory motion.

5. Conclusion

We proposed a method for non-rigid registration on dynamic data. We combined 2D MRI images with physics-based simulation to provide a 3D representation of the liver during breathing motion. As future work we first plan to perform a quantitative evaluation of the compliance and its influence on the simulation; the main objective would be to find the optimal value to drive the simulation. In addition, we will implement the method to work with a single dynamic constraint, so that registration could be performed on ultrasound images.

References

[1] S. Abdelaziz, L. Esteveny, P. Renaud, B. Bayle, L. Barbé, M. De Mathelin, and A. Gangi. Design considerations for a novel mri compatible manipulator for prostate cryoablation. *International Journal of Computer Assisted Radiology and Surgery*, 6(6):811–819, 2011.

[2] E. Coevoet, N. Reynaert, E. Lartigau, L. Schiappacasse, J. Dequidt, and C. Duriez. Introducing interactive inverse FEM simulation and its application for adaptive radiotherapy. In *MICCAI - 17th International Conference on Medical Image Computing and Computer-Assisted Intervention*, Boston, United States, September 2014.

[3] H. Courtecuisse, P. Allard, J.and Kerfriden, S. Bordas, S. Cotin, and C. Duriez. Real-time simulation of contact and cutting of heterogeneous soft-tissues. *Medical image analysis*, 18(2):394–410, 2014.

[4] H. Courtecuisse, I. Peterlik, R. Trivisonne, C. Duriez, and S. Cotin. Constraint-Based Simulation for Non-Rigid Real-Time Registration. In *Medicine Meets Virtual Reality*, Manhattan Beach, California, United States, February 2014.

[5] I. Elgezua, Y. Kobayashi, and M. Fujie. Survey on current state-of-the-art in needle insertion robots: Open challenges for application in real surgery. *Procedia {CIRP}*, 5:94 – 99, 2013.

[6] M Ferrant, a Nabavi, B Macq, F a Jolesz, R Kikinis, and S K Warfield. Registration of 3-D intraoperative MR images of the brain using a finite-element biomechanical model. *IEEE transactions on medical imaging*, 20(12):1384–97, December 2001.

[7] G.Fischer, A.Deguet, C.Csoma, R.Taylor, L.Fayad, J.Carrino, J.Zinreich, and G.Fichtinger. Mri image overlay: Application to arthrography needle insertion. *Computer Aided Surgery*, 12(1):2–14, 2007.

[8] B. Gilles and D. Pai. Fast musculoskeletal registration based on shape matching. In D. Metaxas, L. Axel, G. Fichtinger, and G. Székely, editors, *Medical Image Computing and Computer-Assisted Intervention – MICCAI 2008*, volume 5242 of *Lecture Notes in Computer Science*, pages 822–829. 2008.

[9] N. Haouchine, J. Dequidt, I.Peterlik, E. Kerrien, and M.-O. Berger. Image-guided simulation of heterogeneous tissue deformation for augmented reality during hepatic surgery. In *Proc. of ISMAR, Int. Symposium on Mixed and Augm. Reality*, 2013.

[10] K Masamune, E Kobayashi, Y Masutani, M Suzuki, T Dohi, H Iseki, and K Takakura. Development of an MRI-compatible needle insertion manipulator for stereotactic neurosurgery. *Journal of image guided surgery*, 1(4):242–248, 1995.

[11] M. Müller and M. Gross. Interactive virtual materials. In *GI '04: Proc. of Graphics Interface 2004*, pages 239–246, School of Computer Science, University of Waterloo, Waterloo, Ontario,Canada, 2004.

[12] M Neumann, L Cuvillon, E Breton, and M de Matheli. Evaluation of an image-based tracking workflow with Kalman filtering for automatic image plane alignment in interventional MRI. *Conference proceedings : ... Annual International Conference of the IEEE Engineering in Medicine and Biology Society. IEEE Engineering in Medicine and Biology Society. Annual Conference*, 2013:2968–2971, 2013.

[13] R. Seifabadi, S. Song, A. Krieger, N. Cho, J. Tokuda, G. Fichtinger, and I. Iordachita. Robotic system for mri-guided prostate biopsy: feasibility of teleoperated needle insertion and ex vivo phantom study. *International Journal of Computer Assisted Radiology and Surgery*, 7(2):181–190, 2012.

[14] S. Suwelack, S.and Röhl, S. Bodenstedt, D. Reichard, R. Dillmann, T. dos Santos, L. Maier-Hein, M. Wagner, J. Wünscher, H. Kenngott, B. Müller, and S. Speidel. Physics-based shape matching for intraoperative image guidance. *Med. Phys.*, 41(11):111901, 2014.